Int. J. Nano Dimens., 10 (3): 260-271, Summer 2019

ORIGINAL ARTICLE

Synthesis and characterization of new spinel $Mn_{0.5}Cu_{0.5}Cr_2O_4$ and degradation of Malachite Green from wastewater in comparison with $CuCr_2O_4$

Fatemeh Soleimani[1], Mahdi Salehi[1,] Ahmad Gholizadeh[2]*

[1] *Department of Chemistry, Semnan University, Semnan, Iran.*
[2] *Department of Physics, Damghan University, Semnan, Iran.*

Received 24 December 2018, revised 25 March 2019, accepted 29 March 2019, available online 30 March 2019

Abstract

In this study phase- pure new spinel structure, $Mn_{0.5}Cu_{0.5}Cr_2O_4$ was prepared by hydrothermal method successfully and the degradation of Malachite green as an organic pollutant was investigated and compared with $CuCr_2O_4$. Purification of obtained nanoparticles was measured by using X-ray diffraction method (XRD) in which crystal structure and the structural properties were studied by using X'Pert package and Fullprof program. Also, the morphology of obtained materials was modified by field-effect scanning electron microscopy (FESEM). These materials were characterized by Fourier-transform infrared spectroscopy (FTIR) and thermogravimetric analysis (TGA), respectively. UV-vis diffuse reflectance analysis was done for determination of band gape which evaluated 1.37eV. The photocatalytic application of synthesized materials was evaluated by the degradation of malachite green (MG) in the presence of H_2O_2 that were assessed by UV–vis spectroscopy analysis. The comparison study of photocatalytic result reviled that $Mn_{0.5}Cu_{0.5}Cr_2O_4$ has higher activity than $CuCr_2O_4$.

Keywords: *$CuCr_2O_4$; Hydrothermal Method; Malachite Green; $Mn_{0.5}Cu_{0.5}Cr_2O_4$; Photocatalytic Activity.*

How to cite this article

Soleimani F, Salehi M, Gholizadeh A.. Synthesis and characterization of new spinel $Mn_{0.5}Cu_{0.5}Cr_2O_4$ and degradation of Malachite Green from wastewater in comparison with $CuCr_2O_4$. Int. J. Nano Dimens., 2019; 10 (3): 260-271.

INTRODUCTION

AB_2O_4 Spinel-type metal oxides are applied in various fields due to their various technological applications and properties. There are two types of cations in a normal spinel structure, A^{2+} and B^{3+}, which A^{2+} ions occupy tetrahedral sites which are surrounded by oxygen and B^{3+} ions occupy octahedral sites which have been surrounded by six oxygens [1, 2]. Copper chromate has been attended due to distinguished electrical, catalytic, magnetic and optical properties in recent years; for example, it is used as versatile catalyst due to its stable structure for oxidation of CO which is widely used in space launch vehicles [3] and hydrogenation process catalyst in oil industries [4, 5]. Also, this chromate is a visible light active photocatalyst with band gap energy of 1.4ev. So, this p-type semiconductor has an extensive range of usages as photocatalyst because according to Shockley-Quiser limit, materials have the most visible light absorption of solar light irradiation in this rang, so this band gap makes it highly activated [6-8].

The most common methods which have been used for synthesizing copper chromate are: hydrothermal [4], co-precipitation [9, 10], sol-gel [11], thermal decomposition [12], solid state [7] and so on. Among these methods, hydrothermal is one of the best methods to fabricate verity morphologies. Also, this method is high efficiency and cost-effective method [13-15]. In this research, the hydrothermal method has been performed because the recent studies show that the photodegradation process by means of $CuCr_2O_4$ has a direct relationship with its morphology [16]. $Mn_{0.5}Cu_{0.5}Cr_2O_4$ is chromate that Mn^{+2} and Cu^{2+} occupy tetrahedral sites

* Corresponding Author Email: *msalehi@semnan.ac.ir*

contemporaneously. This chromate has not been synthesized yet; so, its applications haven't been assessed before.

In this work, we investigate the effect of Mn^{2+}-substituted in spinel structure of $CuCr_2O_4$. At first step, a pure phase of $Mn_{0.5}Cu_{0.5}Cr_2O_4$ was synthesized successfully via hydrothermal method. In the next step, it was tried to assess the photodegradation activity of $Mn_{0.5}Cu_{0.5}Cr_2O_4$ for irradiation a cationic dye (malachite green). Among water pollutant, toxic dye molecules like Malachite green (4-{[4-(dimethylamino) phenyl] (phenyl) methylidene}-N'Ndimethylcyclohexa-25-dien-1-iminium chloride) (MG) which are harmful to the environment, has got more attention these days. The hazardous compound has been widely used in textile industry for the dyeing wool, food coloring and ceramics, so that 1-15% of this dye is distributed during dyeing process and enter to the water [17-19]. So, the removal process of this compound is important from industrial waste water. There are various methods for elimination a variety ranges of pollutants and toxic dyes from contaminating water; one of these processes is chemical oxidation technology which is used in certain semiconductor photocatalyst process and the solar radiation.

One of the most important effective factors on photocatalytic performance is the existence of a powerful source of energy for the excitement of electrons from valence band to conduction band which can create electron-hole pair. This energy should be either equal with or stronger than semiconductor band gap-which is a distance between the conduction band and valance band. The solar light detaches an electron from the photocatalyst surface and creates a hole. This hole can react with OH^- and creates active radicals. As a matter of fact, the progress of these processes regularly depends on production of $O_2^{\bullet-}$ and reactive radicals like $OH^{\bullet}$ that is capable of oxidation organic contaminants. In this study is tried to produce more reactive radicals with assistantship H_2O_2 for improving the photodegradation process [20, 21]. The photocatalyst mechanism of MG degradation has been shown in Fig. 1.

The solar energy is an eco-friendly source of energy that exists on earth surface. This energy contains 46% visible light, 8% ultraviolet light and the 49.4% as infrared radiation, so finding a suitable photocatalyst with the ability of absorbing sun light or having appropriate band gap is important. Another significant factor in the photodegradation process is the size of nanoparticles. So that, electron-hole pair operation is done by absorption of radiation on nanoparticles surface before they recombine with the surface adsorbed species. In smaller particles, the transition of an electron to the surface is easier and need shorter time duration [22, 23].

In this study, the chromates were synthesized by hydrothermal method and the obtained materials were investigated by various methods like FESEM, FTIR, TGA and XRD. At the end the photocatalyst activity of synthesized material were assessed and compared.

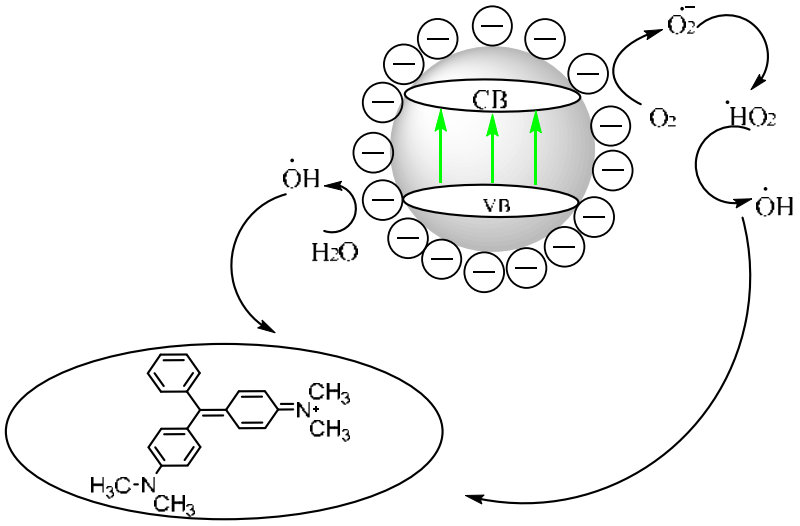

Fig. 1. Photocatalytic mechanism of photodegradation of MG.

EXPERIMENTAL

Materials and methods

All chemical materials were of analytical grade and used without further purification. Phase identifications were performed on a powder X-ray diffractometer D5000 (Siemens AG, Munich, Germany) using CuKα radiation in the range 2θ = 10-90° and the XRD data was analyzed by using X'Pert package and Fullprof program [24]. The morphology of the obtained materials was examined with a field emission scanning electron microscope (Hitachi FE-SEM model S-4160). Fourier-transform infrared spectroscopy (FTIR)was recorded on a Tensor 27 (Bruker Corporation, Germany) in the range 400-4000 cm^{-1}. The thermogravimetric analysis (TGA) has been recorded by STA PT 1600 thermal analysis performed between 25-900°C with the 5°C/min constant rate of heating under an air atmosphere in alumina pan. For controlling photodegradation of Malachite green is used UV–vis diffuse reflectance spectra which were recorded by UV-Visible spectra (Shimadzu UV-1650 PC).

Synthesis of $CuCr_2O_4$ and $Mn_{0.5}Cu_{0.5}Cr_2O_4$

In this method, firstly 1 mmol $Cu(NO_3)_2$ dissolved in 25 mL of distilled water by 15 min stirring. Then, 2 mmol $Cr(NO_3)_2$ was added to the solution and stirred for 15 min again. After that, the solution of 25mL of NaOH (2 M) was added dropwise to achieve pH = 14. In the end, the solution was transferred to the 100 mL Teflon-lined stainless-steel autoclave for hydrothermal treatment at 180°C for 11 h. When the reaction was completed, it was cooled to room temperature. The obtained $CuCr_2O_4$ was washed with deionized water three times to remove impurity and achieve nurture pH. The prepared powder was washed with distilled water and dried at 60 °C for 60 min under normal atmospheric conditions. The obtained powder was added to platinum crucibles and heated in a furnace maintained at 700°C for 5 h. For synthesizing $Mn_{0.5}Cu_{0.5}Cr_2O_4$ was used the same method, but 0.5 mmol $Cu(NO_3)_2$, 0.5 mmol of $Mn(CH_3COO)_2$ and 2 mmol $Cr(NO_3)_2$ were used as initial materials. After solving material, the solution of 25 mL of NaOH (2 M) was added dropwise to receive pH = 14 and heated as same as synthesizing procedure of $CuCr_2O_4$.

Photocatalytic study measurements

Photocatalytic activity of synthesized $Mn_{0.5}Cu_{0.5}Cr_2O_4$ was performed in 100 mL of 10 mg/L Malachite green. The wavelength of the visible part of solar light is between 390 nm to 590 nm so for simulation of this part was used 5 FPL 36W 70LM. The solution was stirred in darkness at room temperature for 45 min for the establishment of adsorption/ desorption between dyes and catalyst. After this time, various amount of H_2O_2 was added to the solution, then 5 mL of suspension was taken as sample after certain interval time and centrifuged (EBA 20 Hettich) with 3500 rpm for removing photocatalyst particles then the absorbance of degraded dye was recorded by spectrophotometer in the range of 200-800 nm, using 1cm quartz cell. Also, it should be considered that Malachite Green has

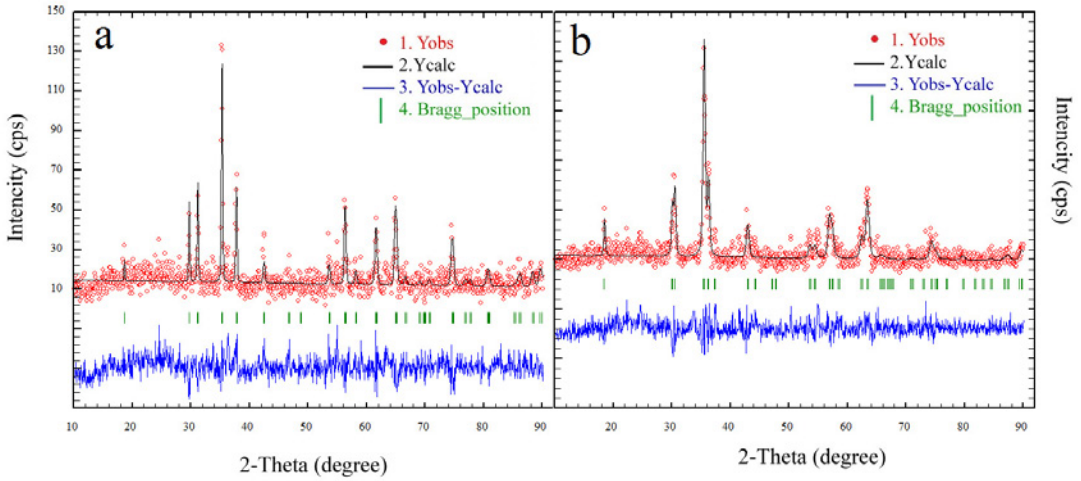

Fig. 2. Calculated PXRD pattern for Rietveld profile of synthesized a) $CuCr_2O_4$ b) $Mn_{0.5}Cu_{0.5}Cr_2O_4$.

high deionization at alkaline pH without the presence of photocatalyst, so the effect of pH was ignored [25].

The efficiency of catalyst performance was calculated commonly by the following equation:

$$\acute{\eta}^{\%} = (\frac{C_i - C_f}{C_i}) \times 100 \quad (1)$$

Where, C_i is the initial concentration of dye (mg L^{-1}) and C_f is residual dye concentration after certain periods (mg L^{-1}).

RESULT AND DISCUSSION

PXRD analysis

The XRD diffraction pattern of synthesized $CuCr_2O_4$ and $Mn_{0.5}Cu_{0.5}Cr_2O_4$ are presented in Fig. 2a and 2b. The investigation of XRD data has been done by X'Pert High Score package and Fullprof program [24]. Identification of crystal structure has been studied by using the X'pert package that confirms the formation of single-phase $Mn_{0.5}Cu_{0.5}Cr_2O_4$. The results demonstrate that all the diffraction peaks of both $CuCr_2O_4$ and $Mn_{0.5}Cu_{0.5}Cr_2O_4$ can be quite well indexed in tetragonal structure (space group I 41/a m d) and the best fit with the least difference is carried out. Complete adaptability and perfect performance in Rietveld refinement require the best amount of initial values and type of space group, which are taken from X'Pert package. The refined lattice parameters, cell volume, specific surface area, density and porosity are summarized in Table 1.

The crystallite size of particles can be calculated by Scherrer's equation:

$$D = 0.94\lambda / \beta \cos\theta \quad (2)$$

In this equation, D show particle size, λ is X-ray wavelength (0.154 nm) and β is broadening at half the maximum intensity of the peak. The largest peak is located at 45.46°. The obtained average crystallite size of synthesized $Mn_{0.5}Cu_{0.5}Cr_2O_4$ nanoparticle is 53 nm.

Another significant factor which is investigated by XRD analysis is Specific Surface Area (SSA). SSA or surface area per unit volume as a material property affects the physical features and chemical reactivity. This factor can be evaluated by measurement of XRD density and particle size and can be calculated according to equation [26]:

$$SSA = \frac{6000}{d\,\rho_{xrd}} \quad (3)$$

Where d is the average size of particle and ρ_{xrd} is the density of synthesized particles that can be estimated by XRD measurement as following relation:

$$\rho_{xrd} = \frac{ZM}{Na^2c} \quad (4)$$

Where Z is the number of atoms in the unit cell (For tetragonal system Z= 4), M is the molecular weight of the samples, N is the Avogadro's constant number, *a* and c are the lattice parameter.

Also, porosity (P) is another factor that can determine the active surface area. This parameter can be calculated by evaluating experimental density by compressing synthesized material and make it as pallet and its difference with theoretical density as following equations:

$$\rho_{exp} = \frac{m}{\pi r^2 h} \quad (5)$$

$$P = \frac{\rho_{xrd} - \rho_{exp}}{\rho_{xrd}} \times 100 \quad (6)$$

Where m is mass of packed powder, r and h are radius and thickness of created pallet. All these parameters are presented in Table 1.

Surface morphology

FE-SEM analysis was used for studying morphology and the size of synthesized materials. Fig. 3 and 4 (a: 2µm, b: 1µm, c: 500nm, d: 200nm) depict various magnificent of synthesized chromates. As could be seen, Fig. 3 reveals that small size particles of $CuCr_2O_4$ uniformly distributed and closely packed and the average size of particles is about 30 nm, also Fig. 4 shows multi-dimensions surface particles of $Mn_{0.5}Cu_{0.5}Cr_2O_4$. The size of the

Table 1. Unit cell parameter, crystallite size, and average grain size for the $Mn_{0.5}Cu_{0.5}Cr_2O_4$.

Sample	*a* (Å)	c (Å)	V(Å^3)	D (nm)	Avg grain size (nm)	ρ_{exp} (g/cm^3)	ρ_{xrd} (g/cm^3)	SSA (cm^2/g)	p
$CuCr_2O_4$	6.015	7.780	281.482	21.94	35	4.72	5.46	31.39	13.55
$Mn_{0.5}Cu_{0.5}Cr_2O_4$	6.008	7.780	280.827	53	90	4.70	5.37	12.41	12.47

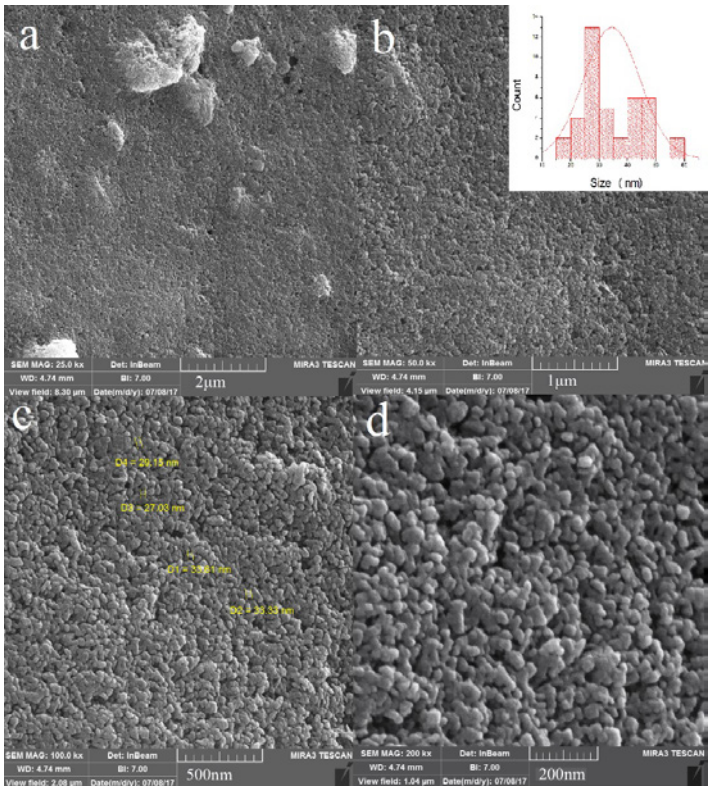

Fig. 3. FE-SEM images of the hydrothermally synthesized $CuCr_2O_4$ (3-a: 2µm, 3-b: 1µm, 3-c: 500nm, 3-d: 200nm).

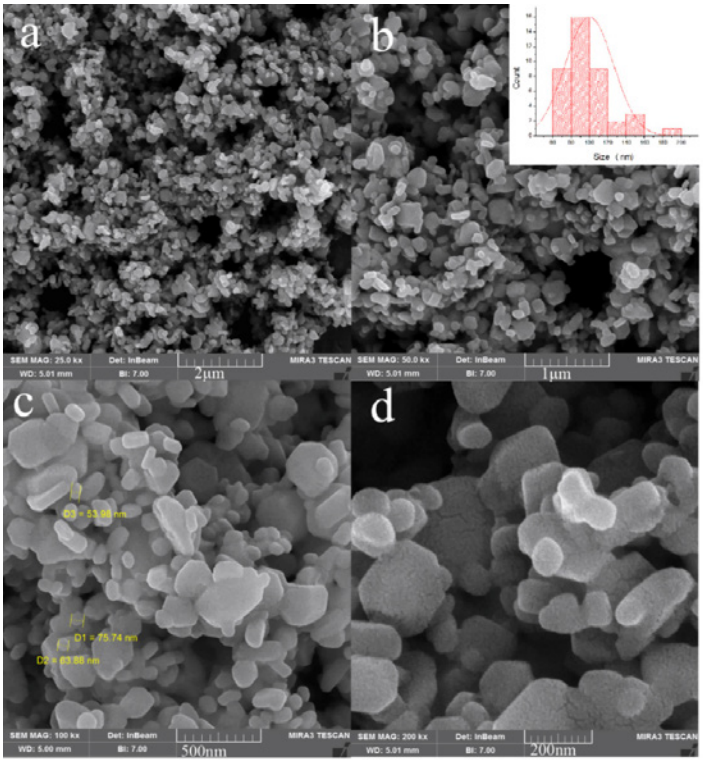

Fig. 4. FE-SEM images of the hydrothermally synthesized $Mn_{0.5}Cu_{0.5}Cr_2O_4$ (4-a: 2µm, 4-b: 1µm, 4-c: 500nm, 4-d: 200nm).

particles is between 30-90 nm. Also, Fig. 5 shows 3D surface topology of $Mn_{0.5}Cu_{0.5}Cr_2O_4$ which was done by Image J software. This image can prove the high surface area of obtained material. The 3D surface morphology is an important factor that can indicate porosity of nanostructures as well and indicates some small bumps to prove high-efficient photocatalyst activity. In recent years, several researches have been done to synthesize semiconductor nanostructures with tunable size and morphology with high surface to volume ratio to effectively degrade contaminant in the environment; synthesized $Mn_{0.5}Cu_{0.5}Cr_2O_4$ is one of those materials. Also, for better comparison should be considered that SSA of P25 is 50 [27].

Fourier transforms infrared spectroscopy (FT-IR) analysis

Figs. 6(a) and 6(b) illustrate the FT-IR spectra of as-prepared $CuCr_2O_4$ and $Mn_{0.5}Cu_{0.5}Cr_2O_4$ respectively; there are two sharp peaks at 520 cm^{-1} and 615 cm^{-1}, which are attributed to stretching vibration mode of Cr-O-Cu, Cr-O and Mn-O. Mn-O stretching vibration mode is overlaid with Cr-O stretching vibration position [28, 29]. Hence high intensity of these peaks refer to the overlay of them with vibration mode of Cr-O-Mn and Cr-O-Cu and confirm synthesis $Cr_2O_4^{-2}$ spinel structure [30]. Also, a peak in the FTIR spectrum at 904 cm^{-1} is attributed to bond bending of H_2O.

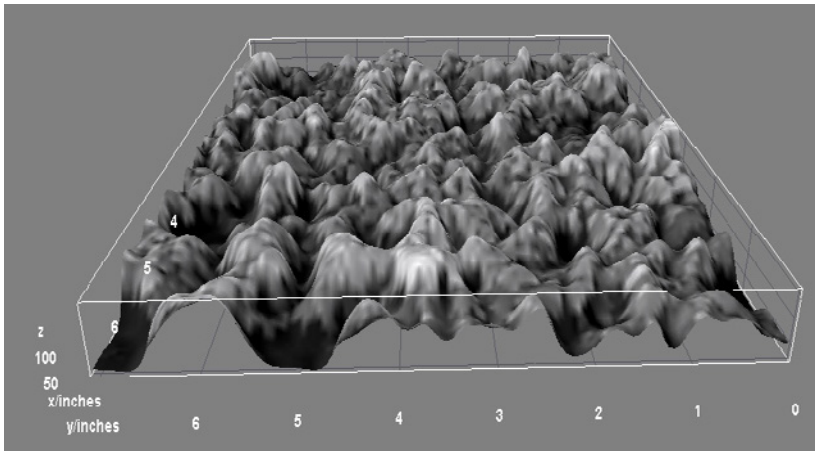

Fig. 5. The3D image of FESEM of the hydrothermally synthesized $Mn_{0.5}Cu_{0.5}Cr_2O_4$.

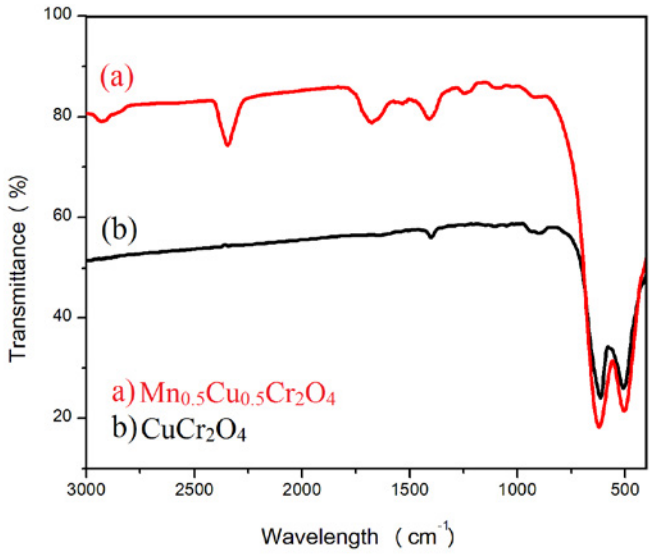

Fig. 6. FT-IR spectra of a)$CuCr_2O_4$ and b)$Mn_{0.5}Cu_{0.5}Cr_2O_4$.

Thermogravimetric analysis (TGA) analysis

Thermogravimetric analysis (TGA) is a technique which determines thermal decomposition behavior of material by gaining weight as a result of increasing temperature and differential thermal analysis (DTA) is a technique usually complete TGA method and is used for calculating heat capacity variations that associated with phase transitions. Fig. 7 shows the TGA curve of as-prepared $Mn_{0.5}Cu_{0.5}Cr_2O_4$ from room temperature to 900°C. The sharp fall at the plot at the beginning up to 130°C belong to the departure of residual water. After that, the sample heated up to 900°C the curve continues with the normal slope which includes no weight loss that emphasizes on the nonexistence of organic material and forming pure crystalline tetragonal phase. After 600° C, the TG curve becomes flat and crystallized $Mn_{0.5}Cu_{0.5}Cr_2O_4$ and only 9.6% weight loss occurs in the temperature range 200-900°C.

UV-vis diffuse reflectance analysis

The band gap energy (E_g) of $Mn_{0.5}Cu_{0.5}Cr_2O_4$ was determined by Tauc model (equation (7)) which is used in semiconductor material commonly.

$$(\alpha h\upsilon)^{1/r} = A(h\upsilon - E_g) \quad (7)$$

Which α is linear absorption coefficient of the material, h is Plank's constant, υ is photon's frequency, A is proportionally constant. E_g is the band gap energy. The value of exponent (r) depends on forbidden or allowed electron

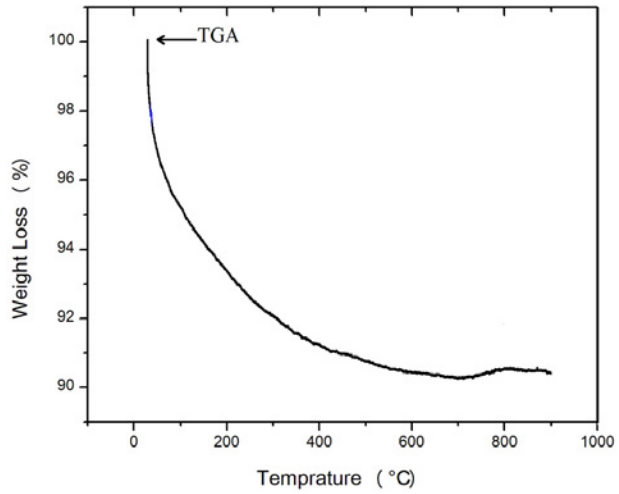

Fig. 7. TGA pattern of $Mn_{0.5}Cu_{0.5}Cr_2O_4$.

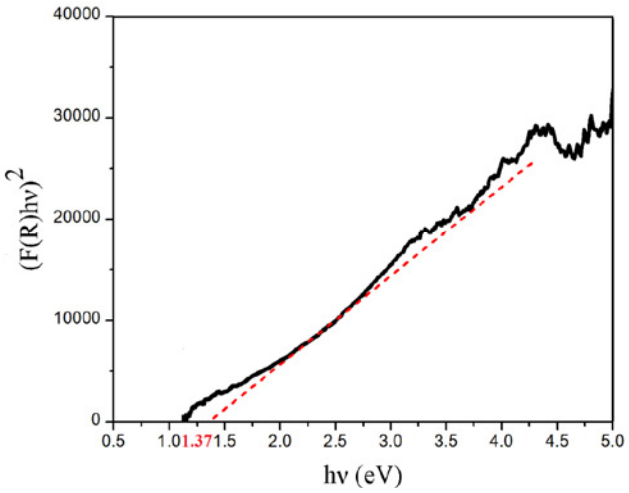

Fig. 8. $(F(R)hv)^2$ versus (hv) Plot for $Mn_{0.5}Cu_{0.5}Cr_2O_4$.

transition that causes to create 4 stats: directly allowed transition (r = 1/2), directly forbidden transition (r = 3/2), indirectly allowed transition (r = 2), indirectly forbidden transition (r = 3). The value of Direct band gap energy can be calculated by using the $(\alpha h\upsilon)^2$ versus hυ plot and extrapolating a straight line on a curve with x-axis [31]. This plot is shown in Fig. 8. The value of band gap for this new chromate is estimated 1.37 eV that almost equal with previous reported of $Cr_2O_4^{-2}$ [32, 33].

Photocatalytic Activity for Degradation of MG in Water

Effect of initial catalyst concentration

In this part the connection between the initial concentration of $Mn_{0.5}Cu_{0.5}Cr_2O_4$ and decolorization of malachite green are showed in various ranges of catalyst in Fig. 9-a and the rate of degradation is illustrated in Fig. 9-b. As it is obvious, the rate of degradation was increased with adding amount of catalyst to a certain amount of catalyst -up to 0.03g- after that, the rate of degradation became stable. That it can be a result of preparation saturated solution.

Reaction kinetics is a part of the chemical reaction which is assessed to give useful data about the speed of reaction rates and the mechanisms of the reactions. In the photocatalytic process, the rate law is used to predict the reaction rate. In a simple chemical reaction, A→B+C, the rate of each part can be evaluated by $R = -\frac{d[A]}{d[t]} = \frac{d[B]}{d[t]} = \frac{d[C]}{d[t]}$. It shows that the decreasing rate of the reactant, lead to an increasing rate of the products reaction also, demonstrates that rate depends on the concentration of the reactants and the rate constant has the unit of 1/s. A total way to demonstrate the reaction rate is to use the power law: rate= $\frac{d[A]}{d[t]} = k[C]^n$, where k is the rate constant and n is the order of the reaction [34, 35].

Theoretically form of rate is:

$$rate = k\left[C_{cat}\right]^m \left[C_{dye}\right]^n \quad (8)$$

This relationship may rely more on the concentration of one particular reactant, and the resulting rate law may include some, all, or none of the reactant species involved in the reaction. So the theoretically rate law can be expressed as equation 8, in which $[C_{cat}]$ is the initial concentration of catalyst, m is reaction order of catalyst concentration, $[C_{dye}]$ is dye concentration and n is reaction order which is depended on dye concentration. In this photocatalytic process the reaction rate is pseudo-first order reaction it means that the catalyst concentration is constant (in this experiment is 0.01 $\%\frac{w}{v}$) the rate of reaction is depended on dye concentration, so the experimental rate constant is:

$$rate = k_{exp}\left[C_{dye}\right]^n \quad (9)$$

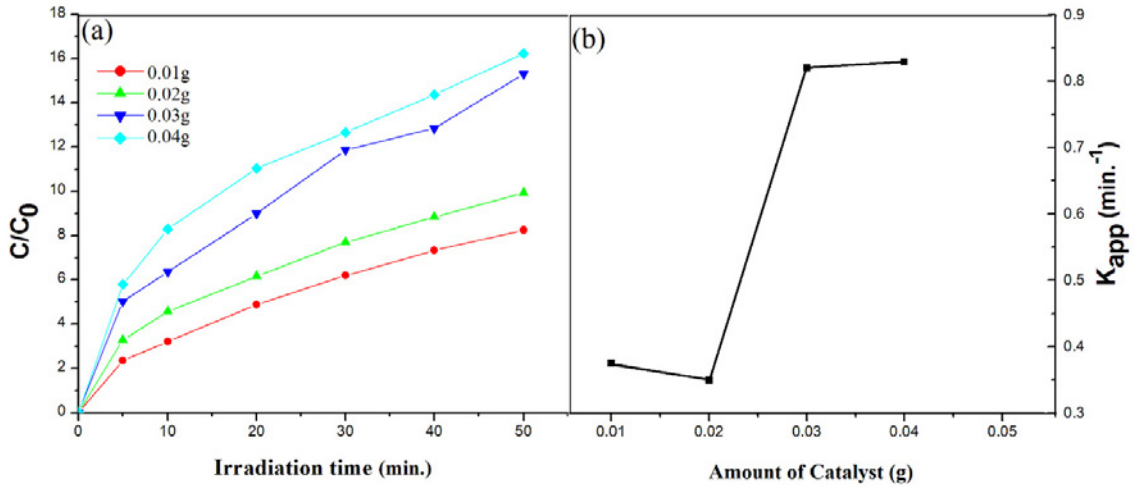

Fig. 9. (a) The effect of initial concentration of $Mn_{0.5}Cu_{0.5}Cr_2O_4$ on photodegradation of Malachite Green. (b) Kinetics data of photocatalytic degradation. Dye concentration = 10 mg L^{-1}, T=298K, H_2O_2=0.1mL.

So, the reaction is the pseudo-first order reaction as follows:

$$-\ln\frac{[C]}{[C_0]} = k_{exp}t \quad (10)$$

Fig. 9-b, demonstrates kinetic study of the initial concentration of photodegradation reaction of $Mn_{0.5}Cu_{0.5}Cr_2O_4$, this data can provide applied and significant information regarding the mechanism of photodegradation and reaction process [36]. Photodegradation of MG in various concentrations 0.01g, 0.02g, 0.03g and 0.04 are 0.3752, 0.3499, 0.8202 and 0.8289 min^{-1}

Effect of H_2O_2

In this part, the relation between the initial amount of H_2O_2 as a parameter with degradation ability and decolorization rate of malachite green is shown in Fig. 10(a). This part is done to investigate the role of H_2O_2 on photodegradation. This diagram which is a pseudo-first-order kinetic curve, establish the effect of initial H_2O_2 on photodegradation. As can see in Fig. 10(*a*), increase in initial H_2O_2, lead to decrease in dye concentration, slightly. The positive effect of H_2O_2 may have two reasons, first photolysis of H_2O_2 to •OH– which is one of the dye degradation accelerators- second reason may refer to the oxidative ability of H_2O_2, Fig. 10-b determine the pseudo-first order rate constants of $CuCr_2O_4$ for photodegradation of MG in various concentrations.

Effect of reactive oxidative species

In this part, the influence of initial reactive species is evaluated by scavenger experiments that are assessed to identify reactive species in the photodegradation process, respectively. The effect

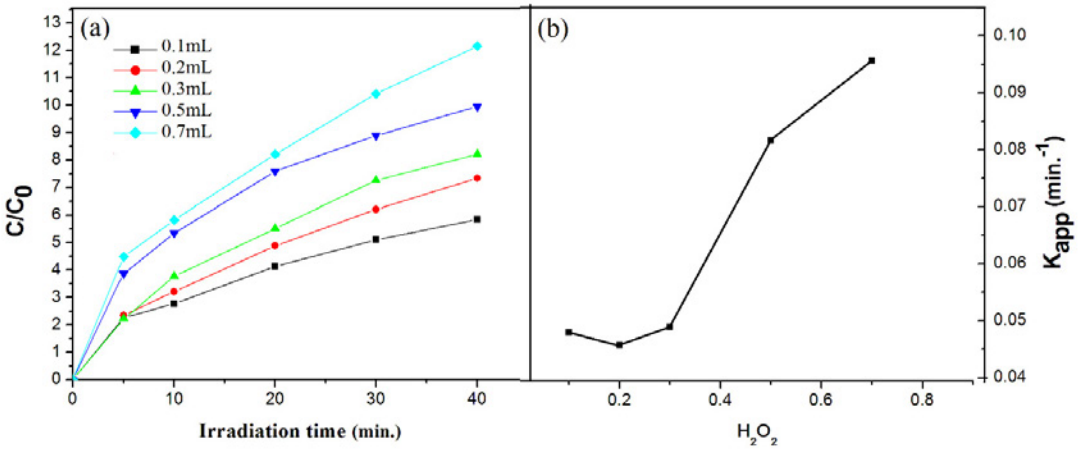

Fig. 10. (a) The effect of H_2O_2 on photodegradation of Malachite Green. (b) Kinetics data of photocatalytic degradation. Dye concentration = 10 mg L^{-1}, T=298K, initial amount of catalyst=0.01g.

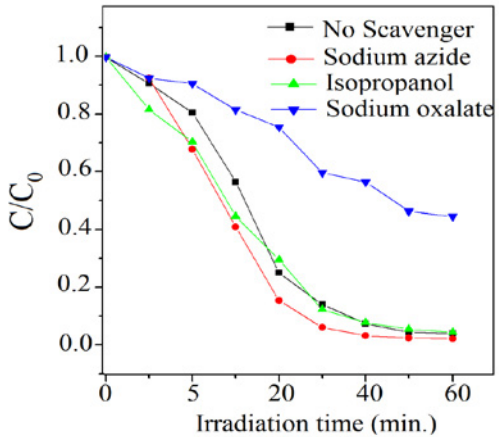

Fig. 11. Photocatalytic degradation efficiency with different scavengers MG, dye concentration = 10 mg L^{-1}, catalyst suspension = 0.01 g, 10 mM NaN_3,10 mM isopropanol, 10 mM sodium Oxalate.

of scavengers on the degradation of MG is shown in Fig. 11. Adding 10mM Azide is used to scavenge $O_2^{\bullet-}$, that cause to increase the degradation rate slightly in target dye that is referred to the formation of superoxide radical. h^+ is another important parameter in photocatalytic degradation, for carrying out its effect, oxalate ion was added to quench h^+. As it is obvious, it has decreased the rate of photodegradation on this process. Also, isopropanol was added for evaluating $^{\bullet}OH$ on photodegradation. Here, $^{\bullet}OH$ could facilitate photocatalytic degradation as well as $O_2^{\bullet-}$.

Fig. 12 demonstrate and compare the photodegradation ability of $CuCr_2O_4$ and $Mn_{0.5}Cu_{0.5}Cr_2O_4$. This comparison shows that the photocatalytic activity of $Mn_{0.5}Cu_{0.5}Cr_2O_4$ is better than $CuCr_2O_4$. This result has a direct relationship with morphology and surface area which is one important factor in photodegradation process; it seems that agglomeration morphology of $CuCr_2O_4$ leads to create lower activated surface so that, has less photodegradation ability. In the other side, $Mn_{0.5}Cu_{0.5}Cr_2O_4$ sample has lower total electronegativity than $CuCr_2O_4$ that it can effect on band gap, so easier electron transition between the conduction band and the valence band [37].

Reusability of photocatalyst

At the last part, the reusability of $Mn_{0.5}Cu_{0.5}Cr_2O_4$ was investigated in three cycles in Fig. 13. Reusability of the catalysts is one of the most important factors which make them useful and economical catalysts. So, checking the recyclability is an essential test [38]. Higher photocatalytic activity

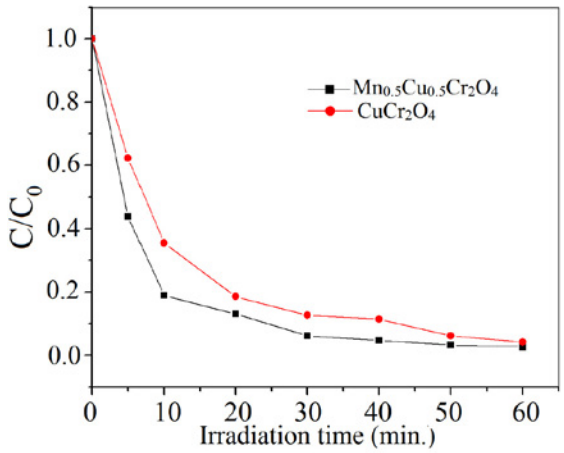

Fig. 12. Comparison between $CuCr_2O_4$ and $Mn_{0.5}Cu_{0.5}Cr_2O_4$ performance in degradation of MG pollutant after 1h irradiation. Dye concentration = 10 mg L^{-1}, T=298K, initial amount of catalyst = 0.01g, H_2O_2 =0.1cc.

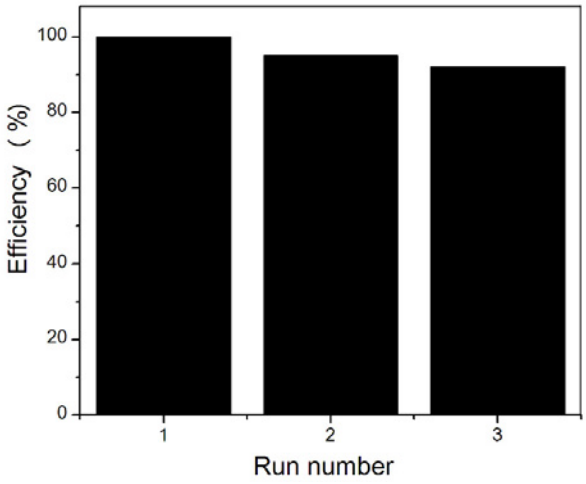

Fig. 13. Reusability of $Mn_{0.5}Cu_{0.5}Cr_2O_4$.

Table 2. Comparison study of the photocatalytic degradation of the $Mn_{0.5}Cu_{0.5}Cr_2O_4$ with other metal oxide.

	catalyst	condition	yield	reference
1	$Mn_{0.5}Cu_{0.5}Cr_2O_4$	10ppm, H_2O_2, 40mg catalyst, 40min,	100	This work
2	$PbCrO_4$	5 ppm ,100mg catalyst, 4 h, pH=7.5, visible light	97	[39]
3	TiO_2/WO_3	5ppm, UVA light,180min	80	[40]
4	TiO_2	40ppm, UV Light, 60min, 20 mg catalyst	100	[41]
5	$Fe_{0.01}Ni_{0.01}Zn_{0.98}O$/polyacrylamide	Solar light, 5mg catalyst, 120min, 5ppm	96	[42]
6	polyaniline/ZnO	Solar light, 0.4mg,10h,5ppm	95	[43]
7	Bi_2WO_6	100mg, pH=2, 30min,10ppm	98	[17]
8	TiO_2−SiO_2	UV light, H_2O_2, Fe^{2+}, 400 ppm catalyst, 5 ppm MG, 25 min, pH=3	97	[44]

of $Mn_{0.5}Cu_{0.5}Cr_2O_4$ leads to higher recyclability which is demonstrated in Fig. 13. The yield of the product approximately decreases by less than 8 percent after three successive cycles. This fact indicates that the possibility of photochemical activity of the catalyst is more than adsorption as result of activated surface. If the degradation had been done by adsorption process, the reusability of catalyst would have decreased rapidly as a result of obstruction of active sites.

Table 2 compare the efficiency of the obtained new synthesized spinel as a photocatalyst and other reported metal oxides in decolorization of MG for more illustration. As it is seen, the ability of degradation by considering time, pH and amount of catalyst for $Mn_{0.5}Cu_{0.5}Cr_2O_4$ nanoparticle in comparison with other reported catalysts is undeniable.

CONCLUSION

In this study, the pure phase of new spinel structure, $Mn_{0.5}Cu_{0.5}Cr_2O_4$, has been synthesized via hydrothermal method. The band gap energy of obtained new material was evaluated 1.37eV which is almost the most effective visible light absorption. The photocatalytic performance of synthesized material for photodegradation of MG was investigated and demonstrated excellent dye photodegradation activity of as-prepared $Mn_{0.5}Cu_{0.5}Cr_2O_4$ that was about 100% after 40min. This issue refers to the appropriate band gap and high specific surface area. Also, the reusability of the synthesized catalyst was investigated and indicated that only 8 percent of the degradation decreased after three successive cycles that this issue clarify priority of photocatalyst activity than adsorption.

ACKNOWLEDGMENT

This work was financially supported by Chemistry department, Semnan University of Iran and the author gratefully thank to their cooperation.

CONFLICT OF INTEREST

The authors declare that there are no conflicts of interest regarding the publication of this manuscript.

REFERENCES

1. Paul B., Bhuyan D., Purkayastha D. D., Dhar S. S., Behera S., (2015), Facile synthesis of spinel $CuCr_2O_4$ nanoparticles and studies of their photocatalytic activity in degradation of some selected organic dyes. *J. Alloys. Compd*. 648: 629-635.
2. Wang Y., (2013), Structure and electrical conductivity of Mn-Based spinels used as solid oxide fuel cell interconnect coatings. 95: 82-85.
3. Prasad, R., Singh P., (2012), A review on CO oxidation over copper chromite catalyst. *Catal. Rev*. 54: 224-279.
4. Acharyya S. S., Ghosh S., Bal R., (2014), Catalytic oxidation of aniline to azoxybenzene over $CuCr_2O_4$ spinel nanoparticle catalyst. *ACS Sustain. Chem. Eng*. 2: 584-589.
5. Lian C., Ren F., Liu Y., Zhao G., Ji Y., Rong H., Jia W., Ma L., Lu H., Wang D., (2015), Heterogeneous selective hydrogenation of ethylene carbonate to methanol and ethylene glycol over a copper chromite nanocatalyst. *Chem. Commun*. 51: 1252-1254.
6. Dollase W., O'Neill H. S. C., (1997), The spinels $CuCr_2O_4$ and $CuRh_2O_4$. *Acta Crystalloger. Sect. C: Cryst. Struct. Commun.* 53: 657-659.
7. Boumaza S., Bouarab R., Trari M., Bouguelia A., (2009), Hydrogen photo-evolution over the spinel $CuCr_2O_4$. *Energ. Convers. Manag*. 50: 62-68.
8. Hu Z. Q., Qin Y., Zhou H. R., Kang J., Zhai S. R., Gao. H., (2011), Preparation and photoelectric properties of $CuCr_2O_4$ nanopowders. *Trans. Tech. Pub. Adv. Mater. Res.*32: 2959-2964.
9. Premalatha K., Raghavan P., Viswanathan B., (2012), Liquid phase oxidation of benzyl alcohol with molecular oxygen catalyzed by metal chromites. *Appl. Catal. A: General*. 419: 203-209.
10. Beshkar F., Amiri O., Salavati-Niasari M., Beshkar F., (2015), Novel dendrite-like $CuCr_2O_4$ photocatalyst prepared by a simple route in order to remove of Azo Dye in textile and dyeing wastewater. *J. Mater. Sci. Mater. Electron*. 26: 8182-8192.
11. Xiao Z., Xiu J., Wang X., Zhang B., Williams C. T., Su D., Liang C., (2013), Controlled preparation and characterization of supported $CuCr_2O_4$ catalysts for hydrogenolysis of highly concentrated glycerol. *Cat. Sci. Technol.* 3: 1108-1115.
12. Geng Q., Zhao X., Gao X., Yang S., Liu G., (2012), Low-temperature combustion synthesis of $CuCr_2O_4$ spinel

powder for spectrally selective paints. *J. Sol-Gel Sci. Technol*. 61: 281-288.
13. Karlsson M., Deppert K., Karlsson L., Magnusson M., Malm J.-O., Srinivasan N., (2005), Compaction of agglomerates of aerosol nanoparticles: A compilation of experimental data. *J. Nanopart. Res*. 7: 43-49.
14. Talebian N., Jafarinezhad F., (2013), Morphology-controlled synthesis of SnO_2 nanostructures using hydrothermal method and their photocatalytic applications*. Ceram. Intl*. 39: 8311-8317.
15. Shokri A., Mahanpoor K., Soodbar D., (2016), Degradation of. 2-nitrophenol from petrochemical waste water by UV/ $NiFe_2O_4$/. Clinoptilolite process. *Fresenius Env. Bull*. 25: 500-508
16. Yuan W., Liu X., Li L., (2014), Synthesis, characterization and photocatalytic activity of cubic-like $CuCr_2O_4$ for dye degradation under visible light irradiation. *Appl. Surf. Sci*. 319: 350-357.
17. Chen Y., Zhang Y., Liu C., Lu A., Zhang W., (2012), Photodegradation of malachite green by nanostructured Bi_2WO_6 visible light-induced photocatalyst. *Int. J. Photoenergy*. 2012: Article ID 510158, 6 pages.
18. Shokri A., Joshagani A. H., (2016), Using microwave along with TiO_2 for degradation of 4-chloro-2-nitrophenol in aqueous environment. *Russ. J. Appl. Chem.* 89: 1985-1990.
19. Shokri, A. and K. Mahanpoor, (2017), Degradation of ortho-toluidine from aqueous solution by the TiO_2/O_3 process.*Int. J. Indust. Chem.* 8: 101-108.
20. Shokri A., (2017), Investigation of UV/H_2O_2 process for removal of ortho-toluidine from industrial wastewater by response surface methodology based on the central composite design. *Desalin. Water. Treat.* 58: 258-266.
21. Shokri A., Rabiee F., Mahanpoor K., (2017), Nanocatalyst (*Mn*/*Iranian hematite*) for *oxidation* of SO2 *pollutant*. in *aqueous* environment. *Int. J. Environ. Sci. Tech.* 14: 2485-2494.
22. Zhang H., Chen G., Bahnemann D. W., (2009), Photoelectrocatalytic materials for environmental applications. *J. Mater. Chem.* 19: 5089-5121.
23. Roonasi P., Mazinani M., (2017), Synthesis and application of barium ferrite/activated carbon composite as an effective solar photocatalyst for discoloration of organic dye contaminants in wastewater. *J. Environ. Chem. Eng*. 5: 3822-3827.
24. Rodrigueg-Carvajal J., (2009), FULLPROF 2000: A program for Rietveld, profile matching and integrated intensity refinements for X-ray and neutron data, version 1.6, *Laboratorie Leon, Brillounin, Gifsuryvette, France*.
25. Fischer A. R., Werner P., Goss K. U., (2011), Photodegradation of malachite green and malachite green carbinol under irradiation with different wavelength ranges. *Chemosphere*. 82: 210-214.
26. Theivasanthi T., Alagar M., (2011), An insight analysis of nano sized powder of jackfruit seed. *ArXiv preprint arXiv:*1110.0346.
27. Hou L., Yang L., Li J., Tan J., Yuan C., (2012), Efficient sunlight-induced methylene blue removal over one-dimensional mesoporous monoclinic $BiVO_4$ nanorods. *J. Anal. Methods Chem.* 2012: Article ID 345247, 9 pages.
28. Madi C., Tabbal M., Christidis T., Isber S., Nsouli B., Zahraman K., (2007), Microstructural characterization of chromium oxide thin films grown by remote plasma assisted pulsed laser deposition. *J. Phys.: Conf. Series.* 59: 600-604.
29. Munawar K., Mansoor M. A., Basirun W. J., Misran M., Huang N. M., Mazhar M., (2017), Single step fabrication of CuO–MnO–2TiO_2 composite thin films with improved photoelectrochemical response. *RSC Adv*. 7: 15885-15893.
30. Mobini S., Meshkani F., Rezaei M., (2017), Surfactant-assisted hydrothermal synthesis of $CuCr_2O_4$ spinel catalyst and its application in CO oxidation process. *J. Environ. Chem. Eng.* 5: 4906-4916.
31. Viezbicke B. D., Patel S., Davis B. E., Birnie D. P., (2015), Evaluation of the Tauc method for optical absorption edge determination: ZnO thin films as a model system. *physica Satus Solidi (b)*. 252: 1700-1710.
32. Mageshwari K., Sathyamoorthy R., Lee J. Y., Park J., (2015), Novel $CuCr_2O_4$ embedded CuO nanocomposites for efficient photodegradation of organic dyes. *Appl. Surf. Sci.* 353: 95-102.
33. Boumaza S., Bouarab R., Trari M., Bouguelia A., (2009), Hydrogen photo-evolution over the spinel $CuCr_2O_4$. *Energy Convers. Managem.* 50: 62-68.
34. Pilling M. J., Seakins P. W., *React. Kinet*. 1996: Oxford University Press.
35. Steinfeld J., Francisco J., Hase W., (1998), Chemical Kinetics and Dynamics, ; Prenctice Hall, *Eng. Sci. Math.: New Jersey*.
36. Reveendran G. A. P., Ong S.-T., (2018), Application of experimental design for dyes removal in aqueous environment by using sodium alginate-TiO_2 thin film. *Chem. Data. Collect.*. 15-16: 32-40.
37. Liu G., Niu P., Sun C., Smith S. C., Chen Z., Lu G. O., Cheng H.-M., (2010), Unique electronic structure induced high photoreactivity of sulfur-doped graphitic C_3N_4. *J. Am. Chem. Soc.* 132: 11642-11648.
38. Soleimani F., Salehi M., Gholizadeh A., (2019), Comparison of visible light photocatalytic degradation of different pollutants by (Zn, Mg)xCu1-xBi_2O_4 nanoparticles. *Ceram. Int.* 45: 8926-8939.
39. Ameta K., Tak P., Soni D., Ameta S. C., (2014), Photocatalytic decomposition of malachite green over lead chromate powder. *Sci. Rev. Chem. Commun.* 4: 38-45.
40. Bojinova A., Dushkin C., (2011), Photodegradation of malachite green in water solutions by means of thin films of TiO_2/WO_3 under visible light. *React. Kinet. Mech. Cat*. 103: 239-250.
41. Soni H., Kumar N., Patel K., Kumar R., (2014), UV light induced photocatalytic degradation of malachite GREEN on TiO_2 nanoparticles. *Int. J. Recent Res. Rev*. 7: 10-15.
42. Kant S., Pathania D., Singh P., Dhiman P., Kumar A., (2014), Removal of malachite green and methylene blue by $Fe0_{.01}Ni_{0.01}Zn_{0.98}O$/polyacrylamide nanocomposite using coupled adsorption and photocatalysis. *Appl. Catal. B: Environ*. 147: 340-352.
43. Eskizeybek V., Sarı F., Gülce H., Gülce A., Avcı A., (2012), Preparation of the new polyaniline/ZnO nanocomposite and its photocatalytic activity for degradation of methylene blue and malachite green dyes under UV and natural sun lights irradiations. *Appl. Catal. B: Environ*. 119-120: 197-206.
44. Eskandarloo H., Badiei A., Behnajady M. A., Mohammadi Ziarani G., (2016), Hybrid homogeneous and heterogeneous photocatalytic processes for removal of triphenylmethane dyes: Artificial neural network modeling. *CLEAN–Soil. Air. Water*. 44: 809-817.